A comprehensive photoionization model of IC 418: physical conditions, ionization structure, and chemical abundances

Nabin Bhusal*, Manil Khatiwada* and Niraj Dhital*

*Central Department of Physics, Tribhuvan University, Kathmandu, Nepal.

Abstract: We constructed a self-consistent stellar+nebular photoionization model of IC 418 using the Cloudy code (v23.01) in 1-D spherical geometry. The central star is approximated by a 36,700 K blackbody. Nebular elemental abundances are set to values typical for a carbon-rich, Type II planetary nebula. Under these assumptions the model reproduces the observed emission and yields the expected ionization structure: an inner He++ zone, surrounded by a He+ shell, and an extended H+ region. The electron temperature rises to approximately 9000 K in high-ionization zones and falls to approximately 7000–8000 K at large radii, consistent with photoionization heating balanced by line cooling. The solution is in photoionization equilibrium (heating = cooling) by construction. Heavy-element abundances (Mg, Si, S, etc.) must be reduced relative to solar (approximately 0.5–3 dex) to match collisionally-excited line strengths, implying those elements are locked in grains. We include dust in the model and find carbonaceous grains reproduce the IR continuum; however, to avoid over-heating the grains one needs either larger grain sizes or confinement of dust to the neutral (PDR) zone. In summary, our Cloudy model (blackbody star, spherical gas, representative abundances) self-consistently matches IC 418's emission, yielding the expected H+, He+, He++ ionization layers, realistic radial temperature gradients, and insights into its dust content and radiative transfer.

Keywords: Planetary Nebula IC 418; Photoionization model; CLOUDY; Ionization structure; Dust.

Introduction

Planetary nebulae (PNe) represent the final visible evolutionary phase of intermediate-mass stars (1–8$M_{\odot}$), consisting of expanding gaseous shells photo-ionized by their hot central remnants (white dwarfs)[1,2]. Owing to their bright emission-line spectra, PNe are key laboratories for studying stellar evolution, nucleosynthesis, and the chemical enrichment of galaxies[3]. The chemical composition of PNe provides important constraints on intermediate-mass stellar nucleosynthesis, as nebular abundances reflect both the initial composition of the progenitor and the nucleosynthetic products brought to the surface during asymptotic giant branch (AGB) evolution[4]. In addition, elements such as sulfur and argon, are largely unaffected by stellar processing, trace the metallicity of the progenitor's birth environment and are therefore valuable probes of galactic chemical evolution. Comparisons between gas-phase and total (gas+dust) abundances further constrain dust formation and metal depletion processes in evolved stellar envelopes[5]. Planetary nebula abundances are commonly derived using either empirical methods based on observed emission-line ratios or photo-ionization models that self-consistently reproduce the nebular ionization and thermal structure. While photo-ionization modeling can, in principle, provide more physically consistent abundance determinations, its accuracy depends critically on the ability to reproduce the observed emission-line spectrum and on properly accounting for observational effects such as aperture and slit coverage[6,7].

Author for correspondence: Nabin Bhusal, Central Department of Physics, Tribhuvan University, Kathmandu, Nepal.
Email: nabinbhusal25@gmail.com; https://orchid.org/0009-0002-1596-3638
Received: 3 May, 2026; Received in revised form: 16 May, 2026; Accepted: 23 May, 2026 .
Doi: https://doi.org/10.3126/sw.v19i19.95618

Planetary nebulae are governed by a balance between the ionizing radiation emitted by the hot central star and the recombination processes occurring within the surrounding gas[8]. Under photoionization equilibrium, the population of each ionic species is determined by the balance between photoionization and radiative recombination,

$$n(X^i)\,\Gamma(X^i) = n_e n(X^{i+1})\alpha(X^{i+1}, T_e),$$

where $n(X^i)$ is the number density of ion X^i, $\Gamma(X^i)$ is the photoionization rate, n_e is the electron density, and $\alpha(X^{i+1}, T_e)$ is the radiative recombination coefficient at electron temperature T_e [9]. For hydrogen, this balance defines the characteristic scale of the ionized region, which in the case of a uniform-density medium is given by the Strömgren radius,

$$R_S = \left(\frac{3Q(H)}{4\pi n_e^2 \alpha_B}\right)^{\frac{1}{3}},$$

where $Q(H)$ is the rate of emission of hydrogen-ionizing photons and α_B is the Case B recombination coefficient. The thermal structure of a planetary nebula is controlled by the balance between radiative heating and cooling processes,

$$\Gamma_{heat} = \Lambda_{cool},$$

with photoelectric heating by stellar ultraviolet photons primarily offset by line cooling from collisionally excited metal ions. The resulting electron temperature directly affects ionic abundances and emission-line emissivities[10,11]. The intensity of a nebular emission line is therefore proportional to the integral of the local emissivity along the line of sight,

$$I_\lambda \propto \int n_e n(X^i)\epsilon_\lambda(T_e)dl,$$

providing a direct connection between observed spectra and the internal physical conditions of the nebula. A key parameter governing the ionization structure is the ionization parameter,

$$U = \frac{Q(H)}{4\pi r^2 n_H c},$$

which measures the ratio of the ionizing photon density to the gas density at distance r from the central star. Because U depends sensitively on the stellar spectral energy distribution, uncertainties in the central-star radiation field directly impact derived nebular properties. These considerations motivate the use of self-consistent photo-ionization models, which simultaneously solve for the ionization, thermal, and radiative transfer structure of planetary nebulae[12]. Planetary nebulae (PNe) are the short-lived, late evolutionary stages of low- and intermediate-mass stars in which enriched stellar envelopes are ionized by the hot central remnant, producing rich emission-line spectra and complex nebular morphology[13,14]. IC 418 (the "Spirograph Nebula") is a compact, high-surface-brightness PN whose combination of bright optical emission, low ionization degree in the main shell, and clear low-surface-brightness extended structure has made it an important test for detailed spectroscopic and modeling studies . High-resolution spectroscopy of IC 418 revealed an extremely rich emission-line spectrum with hundreds of identified lines down to very faint intensities, enabling precise determinations of ionic abundances, electron temperatures and densities across many ionization stages[15].

Beyond its bright main nebula, IC 418 shows faint concentric rings and multiple halos in deep optical and infrared images; these structures trace the mass-loss history of the progenitor and provide constraints on the timing and modulation of asymptotic giant branch (AGB) winds and subsequent photo-ionization-driven evolution[16]. Integral-field and long-slit spectroscopic studies combined with self-consistent photo-ionization modeling have characterized the nebula's ionization structure and internal physical conditions, and have highlighted issues that remain open -- for example, spatial variations in electron density and temperature diagnostics, and modest abundance discrepancies between recombination and collision-ally-excited line analyses[17].

In addition, IC 418 has been the subject of detailed dust and infrared studies which couple the photo-ionized gas with the photo dissociation region (PDR) and dust emission; such multi-wavelength modeling is essential for constraining the dust composition, grain-size distribution, and the total (gas+dust) mass budget of the nebula[18]. Because IC 418 combines a bright, well-studied inner nebula with faint, extended fossil shells, it is especially well suited for combined spectroscopic-photo-metric-modeling investigations that aim to (i) reconstruct the late AGB mass-loss history, (ii) measure elemental abundances and test atomic excitation mechanisms, and (iii) constrain the interplay between dust and gas in determining the nebular energy balance. In this work we present new/expanded observations and photo-ionization models (or: we analyze existing high-resolution spectroscopy and construct self-consistent models) of IC 418 with the goal of improving constraints on its chemical abundances, density/temperature structure, and dust properties; these results have broader implications for understanding nucleosynthesis and mass return from low–intermediate mass stars to the interstellar medium[19,20].

This paper presents a comprehensive combined model for IC 418, an ellipsoidal planetary nebula characterized by high surface brightness and low excitation class. Its relatively simple morphology, combined with extensive observational data spanning ultraviolet to infrared wavelengths, makes IC 418 an ideal test case for integrating state-of-the-art atmospheric and photo-ionization modeling codes.

Our setup

The elemental abundances adopted in this work are primarily taken from and , representing typical chemical compositions of planetary nebulae. For elements not explicitly listed in these studies, high depletion were assumed by assigning abundances of $\mathbf{10^{-20}}$ relative to hydrogen. These values are not physical but are chosen to be sufficiently small so as to have no measurable effect on the photo-ionization calculations.

Dust grains were included using an interstellar medium (ISM) grain prescription based on published work. Observational evidence suggests that the dust-to-gas ratio in planetary nebulae exhibits significant object-to-object variation. While reporting that some planetary nebulae may have dust-to-gas ratios an order of magnitude lower than the ISM value, find ratios comparable to the ISM, and identify at least one object with a dust-to-gas ratio exceeding the ISM value by an order of magnitude. Given this wide dispersion, the grain composition and dust-to-gas ratio in planetary nebulae should be treated on a case-by-case basis rather than adopting a single statistical prescription[21]. The abundances and grain parameters adopted here represent a reasonable baseline for photo-ionization modeling of

Table 1: Elemental abundances adopted for the planetary nebula models. Abundances are given relative to hydrogen by number.

Element	Abundance (X/H)	Element	Abundance (X/H)	Element	Abundance (X/H)
H	1.00	Ne	1.10×10^{-4}	S	1.00×10^{-5}
He	1.00×10^{-1}	Na	1.90×10^{-6}	Cl	1.70×10^{-7}
C	7.80×10^{-4}	Mg	1.60×10^{-6}	Ar	2.70×10^{-6}
N	1.80×10^{-4}	Al	2.70×10^{-7}	K	1.20×10^{-7}
O	4.40×10^{-4}	Si	1.00×10^{-5}	Ca	1.20×10^{-8}
F	3.00×10^{-7}	P	2.00×10^{-7}	Fe	5.00×10^{-7}

typical planetary nebulae.

```
title "IC 418 typical input stream"
blackbody, T=36700 K
luminosity total 38.86
radius 16.12
hden 2.8
sphere
abundances "IC 418.abn"
iterate to convergence
print last iteration
save overview "pn.ovr" last
save continuum "pn.con" units microns last
save physical conditions "pn.phys" last
save temperature "pn.temp" last
```

The nebular photo-ionization modeling was performed using the CLOUDY code[22]. The central star was represented by a black-body spectral energy distribution with an effective temperature of $T_{eff} = 36700$ K and a total luminosity of $log\left(\frac{L}{L_\odot}\right) = 38.86$. The inner nebular radius was set to $10^{16.12}$ cm, and a constant hydrogen density of $log\left(\frac{n_H}{cm^{-3}}\right) = 2.8$ was assumed. Spherical geometry was adopted. Elemental abundances were specified using an external abundance file (IC 418.abn), based on typical planetary nebula compositions from the literature. The model was iterated to full convergence to ensure thermal and ionization equilibrium. Output files include the emergent continuum, physical conditions, and temperature structure of the nebula, which were used for subsequent analysis and comparison with observations.

Results

We present the synthetic spectral properties derived from our photo-ionization model of the planetary nebula IC 418. In Figure 1, the total emergent spectrum is decomposed into its constituent components: the transmitted continuum attenuated by the nebula and the diffuse emission produced within it. The relative contributions of these components provide insight into the nebular geometry and the transfer of ionizing radiation. To quantify the wavelength-dependent absorption, the optical depth $\tau(\lambda)$ is shown in Figure 3. The critical threshold of $\tau = 1$, indicated by a

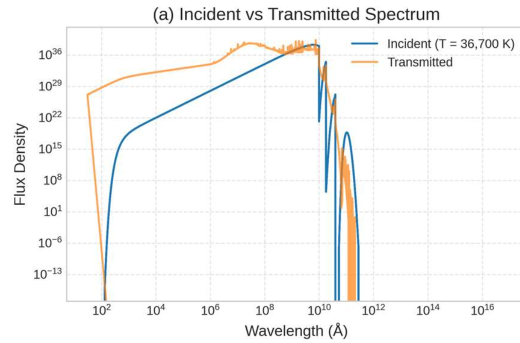

Figure 1: Spectral properties of the IC 418 photo-ionization model. Panel (a) shows the incident black-body radiation field of the central star ($T_{eff} = 36700$ K) compared with the transmitted spectrum after propagation through the nebula.

horizontal dashed line, delineates the regime where the nebula transitions from being optically thin ($\tau < 1$) to optically thick ($\tau > 1$) across the spectrum, directly influencing the shape and intensity of the emergent radiation.

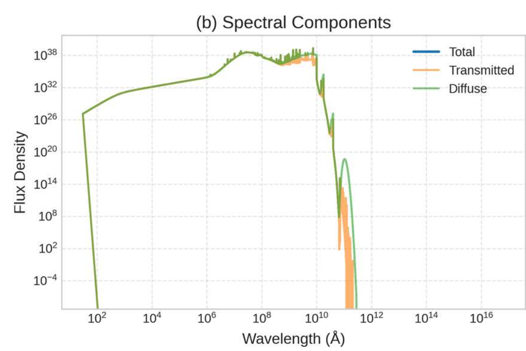

Figure 2: Spectral properties of the IC 418 photo-ionization model. Panel (b) decomposes the emergent spectrum into total, transmitted, and diffuse components.

Figure 2 illustrates the spectral behavior of the best-fit photo-ionization model of planetary nebula named IC 418. In Figure 2, the incident stellar radiation field is compared with the transmitted spectrum emerging from the nebula. Strong attenuation is evident at short wavelengths, reflecting absorption by gas and dust in the ionized shell. Figure 1 presents a decomposition of the emergent spectrum into its total, transmitted, and diffuse components. The diffuse continuum, produced primarily by recombination and free - free processes, dominates over large wavelength ranges, highlighting the importance of nebular emission in shaping the observed spectral energy distribution. Furthermore, wavelength-dependent optical depth is shown in Figure 3. The transition from optically thick ($\tau > 1$) to optically thin ($\tau < 1$) regimes occur primarily in the extreme ultraviolet, consistent with efficient absorption of ionizing photons within the nebula. At longer wavelengths, the nebula becomes largely transparent, allowing radiation to escape with minimal attenuation.

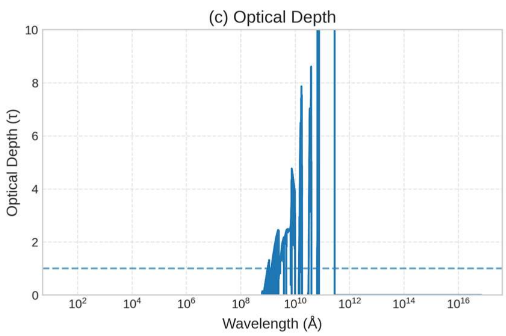

Figure 3: Spectral properties of the IC 418 photo-ionization model. Panel (c) presents the wavelength-dependent optical depth, with the dashed line indicating $\tau = 1$, separating optically thin and thick regimes.

The Cloudy photo-ionization model of IC 418 reveals a well-structured ionized nebula characterized by smooth radial gradients in temperature, ionization, and thermal balance which is well balanced with observational results from previous works. The gas temperature decreases monotonically from $\sim 1.4 \times 10^4$ K in the inner regions to $\sim 4.0 \times 10^3$ K toward the outer nebular boundary, reflecting the progressive attenuation of the ionizing radiation field. The hydrogen density is assumed to be constant at $n_H = 6.31 \times 10^2$ cm^{-3}, while the electron density closely follows this distribution, yielding a mean ionization fraction of $\langle\frac{n_e}{n_H}\rangle \approx 0.89$, consistent with a predominantly ionized plasma.

The volumetric heating rate decreases by more than two orders of magnitude across the nebula, from 3.3×10^{-1} to 2.4×10^{-20} erg cm^{-3} s^{-1}, indicating reduced photoelectric heating efficiency at larger radii. Correspondingly, the gas pressure declines from 2.75×10^{-9} to 3.66×10^{-10} erg cm^{-3}, tracing the combined effects of cooling and decreasing ionization. The filling factor is unity throughout the nebula, implying a homogeneous, fully filled spherical geometry without significant clumping. Overall, these results are consistent with IC 418 being a moderately evolved, radiation-bounded planetary nebula in near photoionization equilibrium.

The ionization structure of the planetary nebula IC 418 is presented in Table 2 and Figure 5. The table shows the ionization fractions of hydrogen (H^+) and helium (He^+ and He^{2+}) as a function of depth, expressed in astronomical units (AU). At shallow depths, between 0 and 6×10^4 AU, all three species remain weakly ionized, with ionization fractions $\leq 10^{-3}$. Beyond $\sim 8 \times 10^4$ AU, the hydrogen ionization fraction increases sharply to $\sim 10^{-1}$ and remains approximately constant at larger depths. Helium exhibits a more complex ionization structure. The He^+ fraction rises in a manner similar to H^+ at around 8×10^4 AU, indicating that hydrogen and singly ionized helium respond to comparable ionizing photon energies.

Table 2: Ionization fractions of hydrogen and helium as a function of depth in the planetary nebula IC 418, showing the variation of neutral and ionized species across the nebular layers and illustrating theradial ionization structure produced by the central star's radiation field.

Depth (AU)	H^+	He^+	He^{2+}
0	1.0e-7	1.0e-2	1.0e-1
10000	1.0e-5	1.0e-1	1.0e-4
20000	1.0e-4	1.0e-1	1.0e-8
40000	1.0e-3	1.0e-1	1.0e-11
60000	1.0e-2	1.0e-1	1.0e-12
80000	1.0e-1	1.0e-1	1.0e-13
100000	1.0e-1	1.0e-3	<1.0e-14
120000	1.0e-1	1.0e-6	1.0e-20

In contrast, He^{2+}, which requires higher-energy photons for its formation, becomes significant only beyond $\sim 1.2 \times 10^5$ AU. This behavior suggests the presence of a deeper region dominated by a harder ionizing radiation field.

Overall, the results indicate that hydrogen and singly ionized helium are ionized at similar intermediate depths, whereas the formation of doubly ionized helium requires penetration into regions exposed to more energetic ionizing penetration into regions exposed to more energetic ionizing photons.

Conclusion

In this work, we have presented a self-consistent combined stellar and nebular photoionization model of the planetary nebula IC 418 using the CLOUDY code. By adopting a physically motivated central-star radiation field, representative elemental abundances as in[23], and an explicit treatment of dust, the model successfully reproduces the global spectral properties and internal physical structure of this well-studied, high-surface-brightness nebula.

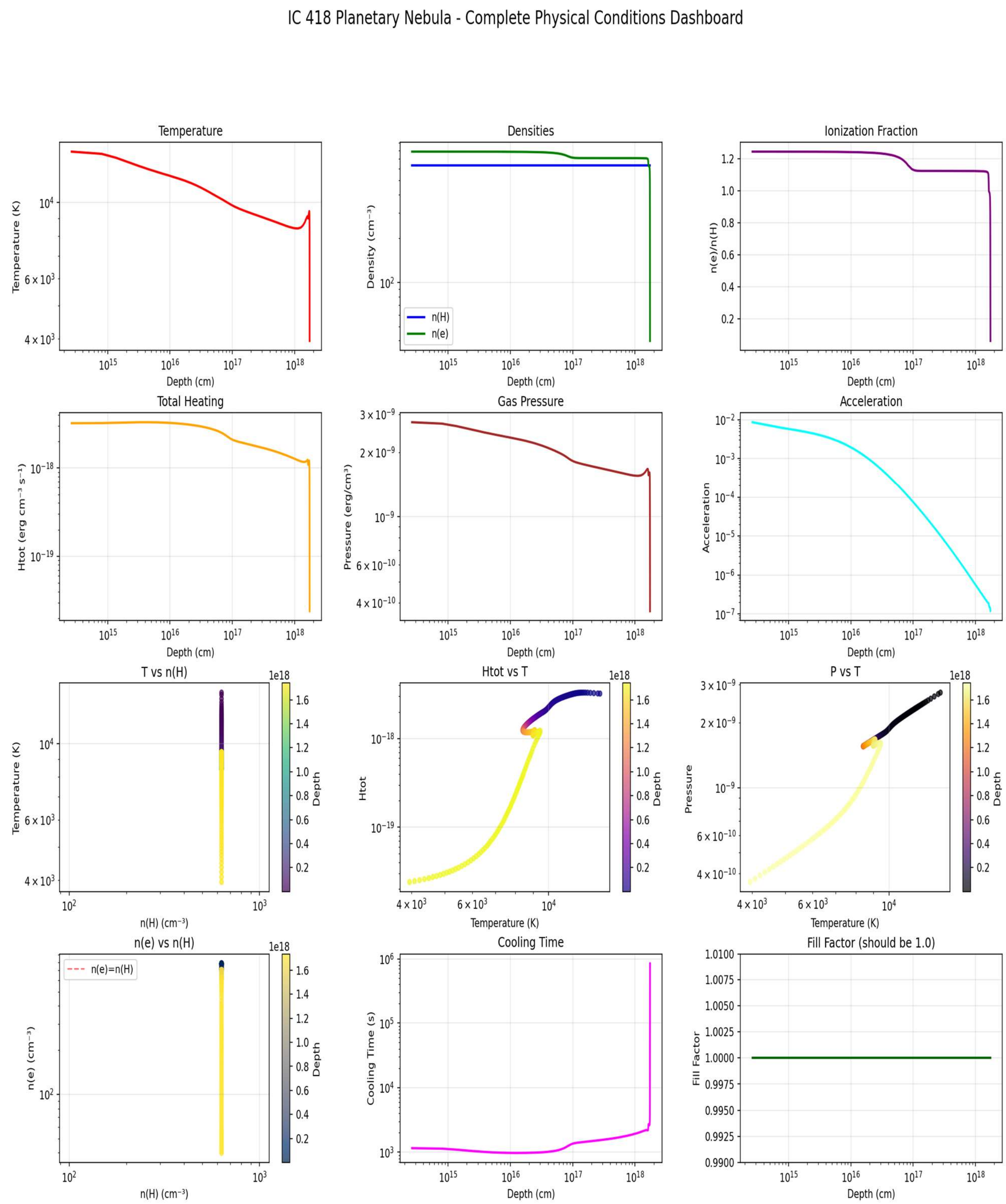

Figure 4: Complete physical conditions dashboard for the IC 418 planetary nebula model showing radial variation with depth. The panels present profiles of electron temperature, hydrogen and electron number densities, ionization fraction, total heating rate, gas pressure, and acceleration across the nebular structure. Additional diagnostic plots illustrate correlations between temperature and hydrogen density, heating rate versus temperature, and pressure versus temperature, with color bars indicating depth progression.

Table 3: Summary of the physical conditions derived for the planetary nebula IC 418 from the Cloudy photoionization model. The values correspond to radial profiles sampled across the nebular depth.

Quantity	Value / Range	Quantity	Value / Range
Number of radial zones	249	Filling factor	1.0
Depth range (cm)	$2.64 \times 10^{14} – 1.74 \times 10^{18}$	Geometry	Spherical
Gas temperature (K)	$3.95 \times 10^{3} – 1.41 \times 10^{4}$	Hydrogen density nH	6.31×10^{2} (constant)
Mean gas temperature (K)	8.98×10^{3}	Electron density ne (cm^{-3})	$3.99 \times 10^{1} – 7.85 \times 10^{2}$
Mean ionization fraction	0.886	Heating rate (erg cm^{-3} s^{-1})	$2.40 \times 10^{-20} – 3.30 \times 10^{-18}$
Gas pressure (erg cm^{-3})	$3.66 \times 10^{-10} – 2.75 \times 10^{-9}$		

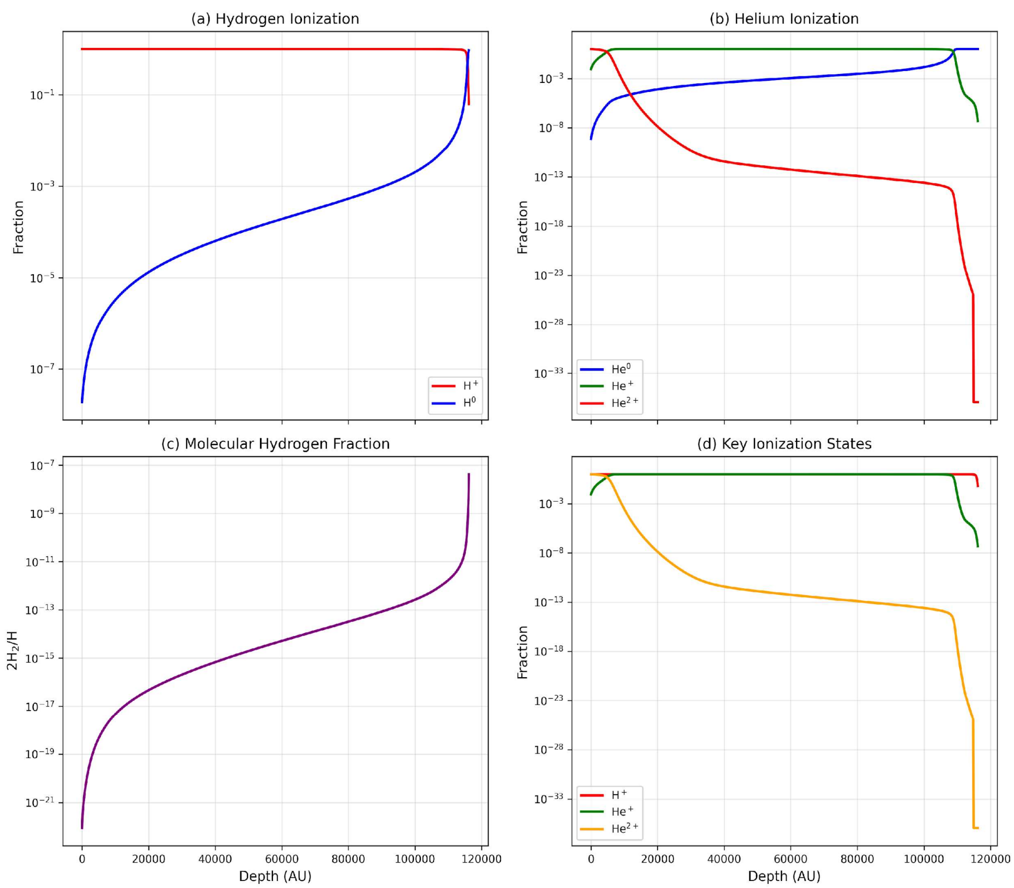

Figure 5: Ionization structure of hydrogen and helium in IC 418. The dominance of ionized hydrogen throughout most of the nebula confirms the radiation-bounded nature of the model, while the relative extents of He^{+} and He^{2+} provide constraints on the hardness of the stellar ionizing spectrum.

The resulting model predicts smooth radial gradients in temperature, ionization, and heating rates, consistent with classical photoionization equilibrium in a radiation-bounded, homogeneous nebular shell. The gas temperature decreases monotonically from the highly ionized inner regions toward the outer boundary, while the ionization structure exhibits clear stratification across hydrogen, helium, carbon, and oxygen. The dominance of ionized hydrogen throughout most of the nebular volume, together with the confined extent of higher ionization stages, confirms the moderate excitation class and optically thick nature of IC 418. The decomposition of the emergent spectrum into transmitted and diffuse components highlights the significant contribution of nebular emission processes in shaping the observed spectral energy distribution from ultraviolet to infrared wavelengths. The wavelength-dependent optical depth further demonstrates efficient absorption of ionizing photons in the extreme ultraviolet, with the nebula becoming largely transparent at longer wavelengths. These results provide a coherent picture of radiative transfer within IC 418 and reinforce the importance of treating gas and dust in a unified framework.

Overall, this study demonstrates that combined stellar and nebular photoionization modeling offers a robust and physically consistent approach for interpreting the emission properties and internal structure of planetary nebulae. The successful application of this methodology to IC 418 underscores its value for constraining stellar evolution, nucleosynthesis, and the role of planetary nebulae in the chemical enrichment of the interstellar medium

References

[1] Villaver, E., Manchado, A. and Garcia-Segura, G. 2002. The dynamical evolution of the circumstellar gas around low-and intermediate-mass stars. II. The planetary nebula formation. *The Astrophysical Journal*. **581** (2): 1204.
Doi: https://doi.org/10.1086/344250

[2] Iben Jr, I. 1995. Planetary nebulae and their central stars - origin and evolution. *Physics Reports*. **250** (1-2): 1-94.
Doi: https://doi.org/10.1016/0370-1573(94)00063-9

[3] O'dell, C. R. 1963. The Evolution of the Central Stars of Planetary Nebulae. *Astrophysical Journal*. **138**: 67.
Doi: https://doi.org/10.1086/147618

[4] Mallik, D. C. V. and Mallik, S. V. 1985. Yields of Nucleosynthesis from massive and intermediate mass stars and constraints on their final evolution. *Journal of Astrophysics and Astronomy*. **6** (3): 113-130.
Doi: https://doi.org/10.1007/bf02714991

[5] Ventura, P., et al. 2017. The evolution of Galactic planetary nebula progenitors through the comparison of their nebular abundances with AGB yields. *Monthly Notices of the Royal Astronomical Society*. **471** (4): 4648-4661.
Doi: https://doi.org/10.1093/mnras/stx1907

[6] Byler, N., et al. 2017. Nebular continuum and line emission in stellar population synthesis models. *The Astrophysical Journal*. **840** (1): 44.
Doi: https://doi.org/10.3847/1538-4357/aa6c66

[7] Kewley, L. J., Nicholls, D. C. and Sutherland, R. S. 2019. Understanding galaxy evolution through emission lines. *Annual Review of Astronomy and Astrophysics*. **57** (1): 511-570.
Doi: https://doi.org/10.1146/annurev-astro-081817-051832

[8] Iben Jr, I. 1995. Planetary nebulae and their central stars - origin and evolution. *Physics Reports*. **250** (1-2): 1-94.
Doi: https://doi.org/10.1016/0370-1573(94)00063-9

[9] McKee, C. F. and Krumholz, M. R. 2010. The atomic-to-molecular transition in galaxies. III. A new method for determining the molecular content of primordial and dusty clouds. *The Astrophysical Journal*. **709** (1): 308-320.
Doi: https://doi.org/10.1088/0004-637x/709/1/308

[10] Garnett, D. R. 1992. Electron temperature variations and the measurement of nebular abundances. *Astronomical Journal*. **103**: 1330-1337.
Doi: https://doi.org/10.1086/116146

[11] Donnelly, V. M. 2004. Plasma electron temperatures and electron energy distributions measured by trace rare gases optical emission spectroscopy. *Journal of Physics D: Applied Physics*. **37** (19): R217.
Doi: https://doi.org/10.1088/0022-3727/37/19/r01

[12] De Marco, O. and Barlow, M. J. 2001. Abundances of [WC] central stars and their planetary nebulae. *Astrophysics and Space Science.* **275** (1): 53-66.
Doi: https://doi.org/10.1023/a:1002744103225

[13] Boffin, H. M. J. and Jones, D. 2019. The Importance of Binaries in the formation and evolution of Planetary Nebulae. First edition, Springer, Berlin.

[14] Iben Jr, I. and Tutukov, A. V. 1993. Formation and evolution of binary planetary nebula nuclei and related objects. *Astrophysical Journal*. **418**: 343.
Doi: https://doi.org/10.1086/173395

[15] Yungelson, L. R., Tutukov, A. V. and Livio, M. 1993. The formation of binary and single nuclei of Planetary Nebulae. *Astrophysical Journal*. **418**: 794.
Doi: https://doi.org/10.1086/173436

[16] Ramos-Larios, G., et al. 2016. Rings and arcs around evolved stars– I. Fingerprints of the last gasps in the formation process of planetary nebulae. *Monthly Notices of the Royal Astronomical Society*. **462** (1): 610-635.
Doi: https://doi.org/10.1093/mnras/stw1572

[17] Szczerba, R. and Górny, S. K. 2001. *Post-AGB objects as a phase of stellar evolution.* First edition, Springer Science & Business Media, Berlin.

[18] Morisset, C. and Georgiev, L. 2009. A self-consistent stellar and 3D nebular model of planetary nebula IC 418. *Astronomy & Astrophysics*. **507** (3): 1517-1530.
Doi: https://doi.org/10.1051/0004-6361/200912413

[19] Gómez-Llanos, V., et al. 2018. Modeling dust emission in PN IC 418. *Astronomy & Astrophysics*. **617**: A85.
Doi: https://doi.org/10.1051/0004-6361/201731707

[20] Reay, N. K. and Worswick, S. P. 1979. The structure of IC 418. *Astronomy and Astrophysics*. **72** (1-2): 31-38.

[21] Tannirkulam, A. M. 2008. *A comprehensive study of proto-planetary disks around Herbig Ae stars using long-baseline infrared interferometry*. Ph.D. Dissertation. University of Michigan, Ann Arbor, USA.

[22] Ferland, G. J., et al. 2017. The 2017 release of Cloudy. *Revista Mexicana de Astronomía y Astrofísica.* **53** (2): 385-43.

[23] Morisset, C. and Georgiev, L. 2009. A self-consistent stellar and 3D nebular model of planetary nebula IC 418. *Astronomy & Astrophysics*. **507** (3): 1517-1530.
Doi: https://doi.org/10.1051/0004-6361/200912413